RSC Advances

PAPER

View Article Online
View Journal | View Issue

Cite this: *RSC Adv.*, 2017, **7**, 31588

In vivo biodistribution and passive accumulation of upconversion nanoparticles in colorectal cancer models *via* intraperitoneal injection†

Yilin Gao,[a] Xingjun Zhu,[a] Yuwen Zhang,[a] Xiaofeng Chen,[b] Li Wang,[b] Wei Feng,[a] Chunhui Huang[a] and Fuyou Li*[a]

Colorectal cancer is a leading cause of death worldwide. Accurate diagnosis and evaluation of malignant extent are crucial for disease treatment. In order to improve the current limited effectiveness of agents for the current theranostics of this disease, we selected upconversion nanoparticles (UCNPs) as an alternative agent, due to their unique luminescence properties. Considering tumorigenesis in the abdominal cavity, intraperitoneal (IP) administration is utilized, based on spatial proximity. Accordingly, citrate-modified UCNPs (cit-UCNPs) were synthesized and injected into mice *via* the IP route, compared with the IV route. The results demonstrated that cit-UCNPs following IP administration encountered significantly different biological processes from those following IV administration. Cit-UCNPs intraperitoneally injected primarily accumulated in the organs in the abdominal cavity, including the pancreas and the mesentery, while the intravenously injected UCNPs mainly gathered in the liver and the spleen. Through the IP route, the majority of cit-UCNPs accumulated in the cancerous cecum tissues, while the minority gathered in the normal cecum tissues. Consequently, cit-UCNPs administrated *via* the IP route to treat colorectal cancer are superior for clinical applications.

Received 18th April 2017
Accepted 2nd June 2017

DOI: 10.1039/c7ra04349j

rsc.li/rsc-advances

1 Introduction

Colorectal cancer is a common disease, with the second highest incidence rate worldwide.[1,2] Clinically, laparoscopic colorectal surgery is the main method for treatment of this disease. Due to weak contrast between the cancerous tissues and the normal tissues, it is difficult to use visual inspection to effectively eliminate cancerous tissues.[3,4] Therefore, it is necessary to develop non-invasive or invasive detection techniques for treatment of this cancer.

Recently, near-infrared (NIR) fluorescence-based theranostics have shown great potential in oncology.[5,6] In particular, lanthanide-doped upconversion nanoparticles (UCNPs) display distinct optical properties, such as conversion of long-wavelength NIR light to short-wavelength light, large anti-Stokes shift, sharp emission, long luminescence lifetime and photostability.[7] Thus, they can exhibit high penetration depth and low autofluorescence background in bio-application. To date, UCNPs have been used in bioimaging, photodynamic therapy, photothermal therapy, and traceable delivery.[8–12] However, for these application, UCNPs are generally administrated *via* the intravenous (IV) route. Upon IV administration, UCNPs undergo opsonisation and sequestration by the mononuclear phagocyte system (including the liver and the spleen).[13–16] Because of the peritoneal-blood barrier, it is low tumour-targeting effectiveness that UCNPs show following IV injection into peritoneal tumour models.

As colorectal tumours are located in the abdominal cavity, intraperitoneal (IP) injection seems to be alternative to deliver UCNPs due to spatial proximity. It has been proved that IP administration allows accumulation of exogenous materials in the abdominal cavity at high concentrations and decreases harmful systemic exposure, compared with IV administration.[17–19] So far, no comprehensive and quantitative studies, which focus on the metabolism of UCNPs *via* IP administration in organisms and their tumour-targeting effectiveness in colorectal cancer, have yet been reported. In order to fill this margin, the representative materials, $NaLuF_4$:20% Yb,1% Tm@$NaLuF_4$, were prepared. Citrates were used for ligand exchange as they are frequently-used chelators with excellent biosafety.[20,21] The related biological process of UCNPs *via* IP injection into mice was subsequently determined.

[a]*Department of Chemistry, State Key Laboratory of Molecular Engineering of Polymers, Institutes of Biomedical Sciences, Collaborative Innovation Center of Chemistry for Energy Materials, Fudan University, Shanghai, P. R. China. E-mail: fyli@fudan.edu.cn*
[b]*Center of Analysis and Measurement, Fudan University, 220 Handan Road, Shanghai 200433, P.R. China*

† Electronic supplementary information (ESI) available: Additional characterizations. See DOI: 10.1039/c7ra04349j

2 Results and discussion

2.1 Synthesis and characterization of $NaLuF_4$:Yb,Tm@$NaLuF_4$ nanocrystals modified with citrates

As shown in Fig. 1, transmission electron microscope images illustrated that $NaLuF_4$:Yb,Tm (Fig. 1a) and $NaLuF_4$:Yb,Tm@$NaLuF_4$ (Fig. 1b) were of uniform size with an average diameter of 12 nm and 21 nm, respectively. The interplanar spacing of 0.51 nm also matched with *d*-spacing of (100) plane of hexagonal phase $NaLuF_4$ (Fig. 1c). Energy dispersive X-ray analysis spectrum was shown in Fig. 1d, which confirmed the presence of Lu, Yb and F in the nanocrystals. In Fig. S1,† X-ray diffraction peaks of core and core–shell UCNPs correlated well with hexagonal structure of $NaLuF_4$ (JCPDS no. 27-0726). No diffraction peaks corresponded with cubic phases or other impurities, indicating successful preparation of pure hexagonal-phase cit-UCNPs *via* the solvothermal method.

To achieve satisfactory dispersion of the nanoparticles in water, citrates were used as surface ligands to replace with the oleic acids (OA) of the as-prepared nanocrystals. As confirmed in the Fourier-transform infrared spectra (Fig. S2†), the bands of OA-UCNPs at 2.856 cm^{-1} and 2.928 cm^{-1} were assigned to the symmetrical (ν_s) and asymmetrical (ν_{as}) stretching vibration of methylene (CH_2) in the long alkyl chain, respectively. In addition, the peak of OA-UCNPs at ν = 3.006 cm^{-1} was attributable to =C–H stretching vibration. However, these three peaks disappeared in the spectrum of citrate-modified UCNPs (cit-UCNPs), demonstrating that $-CH_2-CH_2-$ group was eliminated in the ligand exchange reaction. Also, the peaks at 1.460 cm^{-1} and 1.566 cm^{-1}, corresponding to the symmetrical (ν_s) and asymmetrical (ν_{as}) stretching vibration of –COOH group of OA, respectively, shifted to 1.398 cm^{-1} and 1.599 cm^{-1} in the cit-UCNPs spectrum. As a result, OA ligands were successfully replaced with citrates. Under excitation by a CW 980 nm laser, the nanomaterials in water exhibited two characteristic upconversion luminescence (UCL) emission peaks at 475 nm and 802 nm (Fig. 2), stemming from $^1G_4 \rightarrow {}^3H_6$ and $^3H_4 \rightarrow {}^3H_6$ transitions of Tm^{3+}, respectively.

2.2 Absorption, distribution, metabolism and excretion of cit-UCNPs in normal mice

As shown in Fig. 3a, cit-UCNPs preferentially accumulated in the pancreas (60.56% ID per g Lu^{3+}) and the mesentery (46.27% ID per g Lu^{3+}) at 1 h post-injection. As reported, the pancreas in mice is a thin, membranous gland located in the belly.[22] The accumulation of xenobiotics in such tissues is achieved *via* macrophage uptake by tissue-resident and peritoneal macrophages homing to the pancreas.[23] The mesentery is a double layer of peritoneum in the abdominal cavity.[24] Because of a large number of lymph nodes dispersing in the mesentery, this physiological structure provides a large absorbent surface for cit-UCNPs to localize. Accordingly, significant amount of cit-UCNPs accumulated in the pancreas and the mesentery. Subsequently, the amount of Lu^{3+} in the spleen increased to 36.85% ID per g, while the amount in the pancreas and the mesentery decreased to 39.14% ID per g and 35.52% ID per g, respectively, within 12 h. In addition, unit mass accumulations of Lu^{3+} in the liver, the intestines, the stomach, the reproductive system, the peritoneum and the kidneys were less than 20% ID per g within 240 h. To further validate the quantitative results, UCL bioimaging *ex vivo* was performed. As shown in Fig. S3,† strong UCL signals at 1 h were observed in the pancreas and the liver. UCL intensity then gradually decreased over time. As a comparison, cit-UCNPs at an equivalent dosage were administered *via* IV injection, and the results (Fig. 3b and S3†)

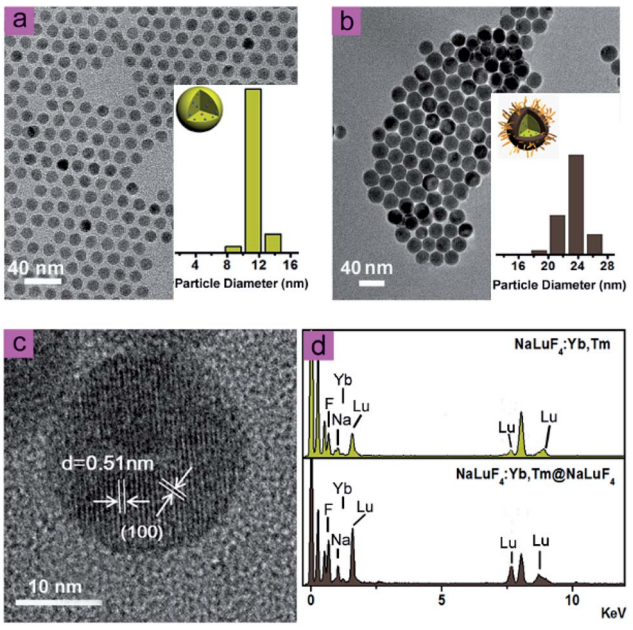

Fig. 1 Characterization of the nanoparticles used in this study. (a) Transmission electron microscope image of $NaLuF_4$:Yb,Tm. (b) $NaLuF_4$:Yb,Tm@$NaLuF_4$ modified with citrates (cit-$NaLuF_4$:Yb,Tm@$NaLuF_4$). (c) High resolution transmission electron microscopy image of cit-$NaLuF_4$:Yb,Tm@$NaLuF_4$. (d) Energy dispersive X-ray analysis spectra of $NaLuF_4$:Yb,Tm and cit-$NaLuF_4$:Yb,Tm@$NaLuF_4$.

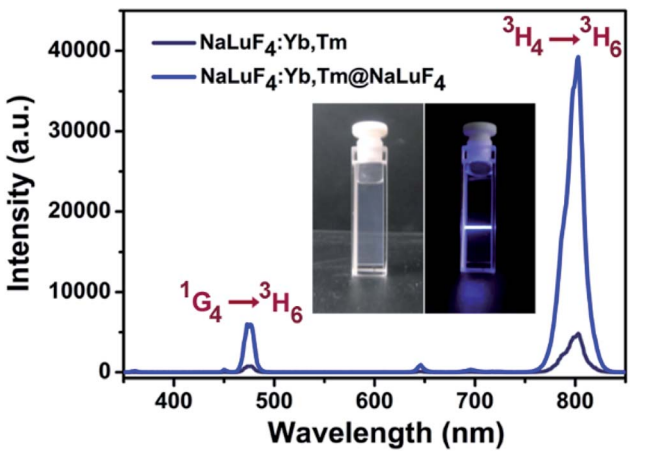

Fig. 2 Upconversion luminescence spectra of $NaLuF_4$:Yb,Tm and $NaLuF_4$:Yb,Tm@$NaLuF_4$ upon excitation at 980 nm. Inset: the bright field and upconversion luminescence photographs of cit-$NaLuF_4$:Yb,Tm@$NaLuF_4$ (2 mg mL^{-1} in deionized water), respectively.

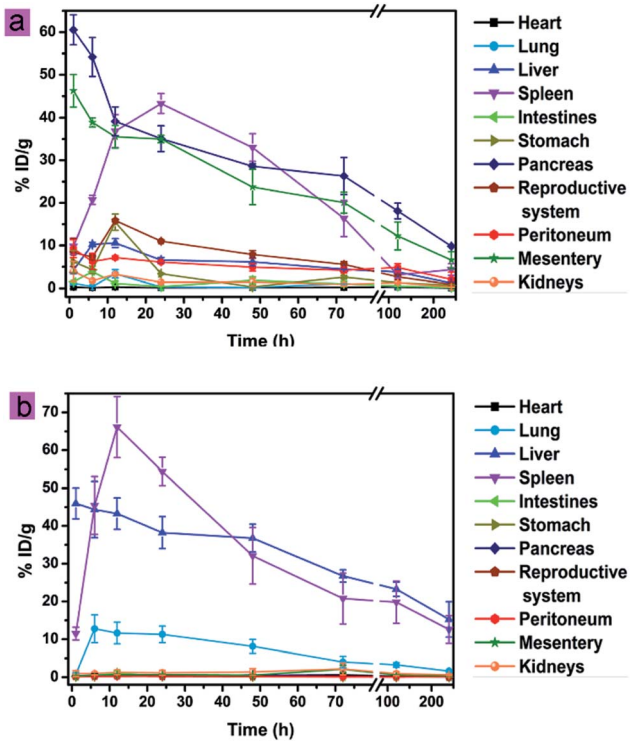

Fig. 3 Unit mass accumulation (% ID per g) of Lu^{3+} in the main tissues at various time points (1 h, 6 h, 12 h, 24 h, 48 h, 72 h, 120 h and 240 h) after intraperitoneal (IP, a) or intravenous (IV, b) injection of cit-$NaLuF_4$:Yb,Tm@$NaLuF_4$ (16 mg kg^{-1} wt) into the normal male mice (n = 3). % ID per g of Lu^{3+} was calculated by comparing the amount of Lu^{3+} in certain tissue per gram with standard of injected dose (ID).

suggested that UCNPs predominantly localized in the liver and the spleen. These results indicated that these two dense organs were dominant mode of clearance for the particles. Because the mass of the liver was usually larger than the mass of the spleen, unit mass accumulations (% ID per g) of cit-UCNPs in the spleen were obviously greater than that in the liver during 6–48 h after IV injection.

Moreover, the biodistribution of cit-UCNPs *in vivo* was also analyzed by plotting the percent of the total administrated Lu^{3+} in each tissue. Shown in Fig. S4,† in the IP group, the accumulating amounts of cit-UCNPs in the liver and the intestines were more than in the other organs within 6 h. Specially, % ID of Lu^{3+} in the liver was the highest in the normal mice injected intraperitoneally during 6–120 h. Furthermore, injected at the same dosage, less nanoparticles were in the liver *via* the IP route than *via* the IV route.

As reported, the injected agents should be eliminated as much as possible at the termination of clinical treatments. As shown in Fig. S5a,† the elimination of accumulated Lu^{3+} in cit-UCNPs *via* IP injection sharply increased within 12 h and then gradually increased. At 12 h, 14.0% of the total injected dose had been excreted *via* the intestines, and at 240 h, 14.9% had been excreted. The amount excreted after IV injection was less within 240 h, indicating that UCNPs *via* IP injection were excreted faster than those *via* IV injection during the same period (Fig. S5b†). In addition, 0.2% particles underwent renal excretion within 240 h after IP administration. Most of the cit-UCNPs injected intraperitoneally were excreted through the intestines.

2.3 UCL confocal imaging of main organs

To determine topical distribution of cit-UCNPs in the regional and local organs, the tissues extracted from the normal male mice at 6 h after IP administration were cut into sections with 5 μm thick and observed under a fluorescence confocal microscopy. As shown in Fig. S6,† UCL signals at 470 nm were mainly detected in the pancreatic duct, the liver, the red pulp of spleen, the mesentery and the surface of the intestines. Following IV injection, UCL signals in the pancreas, the mesentery and the surface of the intestines were undetected at 6 h, but were detected in the liver and the spleen. Therefore, the mechanism of absorption, distribution, metabolism and excretion of UCNPs modified with citrates *via* IP administration was different from those observed *via* IV administration.

2.4 Biosafety assessment of cit-UCNPs at the dosage used for UCL imaging *in vivo*

The effects of cit-UCNPs on the hematological profile at 24 h and 60 d after IP injection were shown in Fig. 4. Significant differences for neutrophil (NEUT) and the percentage of mononuclear macrophage in white blood cells (MONO%) between the experimental group and the control group ($P < 0.01$) were observed, which represented topical inflammation. NEUT and MONO% are common indicators of body's immune response to exogenous substrates, and represent biological self-defense and self-regulation.[25,26] This is a normal physiological phenomenon. With the exception of NEUT and MONO%, no significant differences were found between the two groups in routine blood analysis. Proteins or enzymatic markers of liver and renal function in the experimental groups revealed no significant differences from those in the control groups. In addition, no pathological changes or injuries were detected in main organs following cit-UCNPs administration (Fig. 5). These results reflected biological safety of cit-UCNPs *via* IP injection at the dosage used for NIR fluorescence tracking imaging over a short or long period.

With the respect of theranostic applications of UCNPs, the toxicity of such nanoparticles *in vivo* is indispensable to be concerned. Since UCNPs are delivered into body mainly through intravenous injection, lots of the relate studies concerning the long-term toxicity of UCNPs have been reported so far. For example, triplet–triplet annihilation-based upconversion nanocapsules were injected into mice *via* the intravenous route at the dosage of 1.200 mg kg^{-1} wt, no noticeable toxicity over a period of 60 days was observed with the data of body weight, histological test, hematological test and blood biochemical examination.[14] Polyacrylic acid-coated $NaYF_4$:Yb,Tm nanophosphors (average diameter, 11.5 nm) were intravenously injected into mice at the dosage of 15 mg kg^{-1} wt. Within 115 days following administration, the behaviour, body weight, histology, hematology and serum biochemistry of the mice were analyzed. No abnormal indicators were observed, suggesting

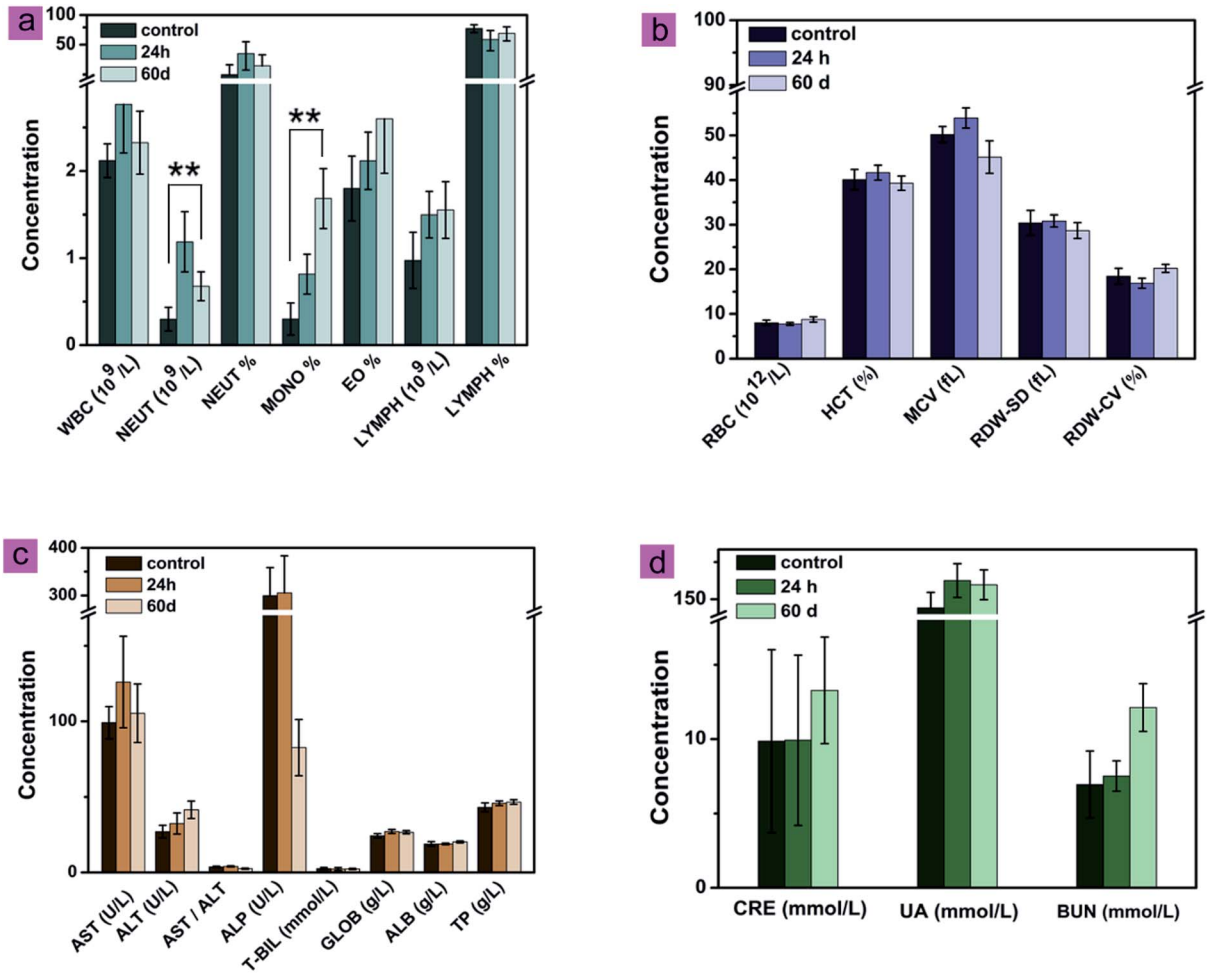

Fig. 4 Routine hematological assay (a and b), and the indices of the liver and renal function (c and d) of the normal male mice at 24 h and 60 d after IP injection with cit-$NaLuF_4$:Yb,Tm@$NaLuF_4$ at a dose of 16 mg kg^{-1} wt ($n = 6$). The mice receiving no injection served as the control ($n = 6$). $^{**}P < 0.01$ *versus* the control.

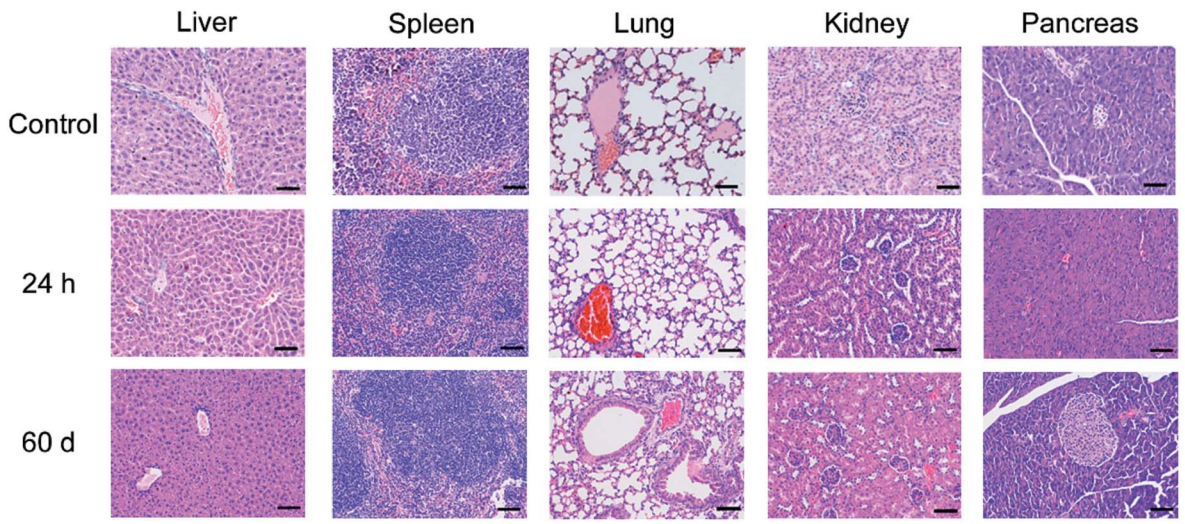

Fig. 5 Histological analysis of the tissues in the normal male mice at 24 h and 60 d after IP injection with cit-$NaLuF_4$:Yb,Tm@$NaLuF_4$ at a 16 mg kg^{-1} wt dosage. The tissues were harvested from the liver, the spleen, the lung, the kidneys and the pancreas. Scale bars represented 50 μm.

that these nanoparticles were biosafe under certain experimental conditions for *in vivo* application.[27] Whereas, the studies about toxicity of UCNPs injected intraperitoneally into body are insufficient. The biosafety results in this study are doubtlessly useful to further application of UCNPs in biomedicine.

2.5 Tumour accumulation of cit-UCNPs in colorectal cancer models

Based on the biodistribution of cit-UCNPs *via* IP injection and satisfactory biological safety, cit-UCNPs seemed to have suitable applications in diagnosis and treatment of abdominal cancer. In order to verify this hypothesis, passive tumour-targeting effectiveness of cit-UCNPs after IP administration was detected. The IP group exhibited excellent results that % ID per g (unit mass accumulations) of Lu^{3+} in cit-UCNPs in the tumours was markedly higher than that in the normal organs after 6 h (Fig. S7a†), while % ID per g of Lu^{3+} in the tumours in the IV group was significantly lower than that in the liver, the spleen and others within 240 h (Fig. S7b†). Within 24 h following IP injection, part of cit-UCNPs gathered in the intestines, resulting in fast excretion in the initial period after administration (Fig. S8a†). At 72 h, % ID of Lu^{3+} in the LOVO tumours in the IP group was the highest. The passive tumour-targeting effectiveness of the intraperitoneally injected cit-UCNPs was higher than the intravenously injected particles (Fig. S8†). The related luminescence imaging of mice in the IP group also validated the quantitative results (Fig. 6), which suggested that passive tumour-targeting effectiveness of cit-UCNPs *via* IP injection was higher than that *via* IV injection. As shown in Fig. 7a, unit mass accumulations of Lu^{3+} in cit-UCNPs in the tumours were more than 20% ID per g within 72–120 h in the IP group, and was less than 2.0% ID per g within 240 h in the IV group. Particularly, at 72 h after administration, 43.20% ID per g of the cit-UCNPs were in the LOVO tumours in the IP group, while 0.60% ID per g of the cit-UCNPs were in the LOVO tumours in the IV group. The former was more 72 times than the later. This result was far superior to the reported active tumour-targeting effectiveness of other materials in the cancer models. As reported, a multifunctional gold-nanoparticle system composed of a monoclonal antibody against epidermal growth factor receptor and a Co(II) coordination compound was intravenous injected into HCT116-derived xenografts tumours, and its accumulating concentration in the tumours was appropriately more 3.62 times than that of the non-targeted counterpart.[28]

Confocal microscopy showed that UCL signals from the tumours in the IP group were positively detected at 1 h and 72 h, and most particles gradually permeated from the exterior to the interior of solid tumours over time (Fig. 7b). In contrast, signals from the tumours in the IV group were not detected at the same time point. These results suggested that the passive tumour-targeting effectiveness of UCNPs *via* IP injection was higher than that *via* IV injection.

The effectiveness of nanoparticle application in cancer theranostics is partly dependent on administration routes. Different administration may lead to significant differences in biodistribution pattern of agents. The clinical administrating ways include oral, intravenous, intraperitoneal, intra-arterial, intra-muscular, and so on. The oral administration can be performed easily, but there are many barriers such as digestive fluids and acidic pH that hamper effective agent delivery.[29] After intravenous administration, the agents *in vivo* always interact with blood components, resulting in large amounts accumulating in the mononuclear phagocyte system (the liver and the spleen).[11] The intraperitoneal administration can increase agent concentration in the peritoneal tumours, on the basis of spatial proximity. The biocompatible agents at high molecular weight exhibit prolonged retention in the abdominal cavity.[17] The intra-arterial administration can deliver agents into the main bloodstream with high concentration.[30] It causes more

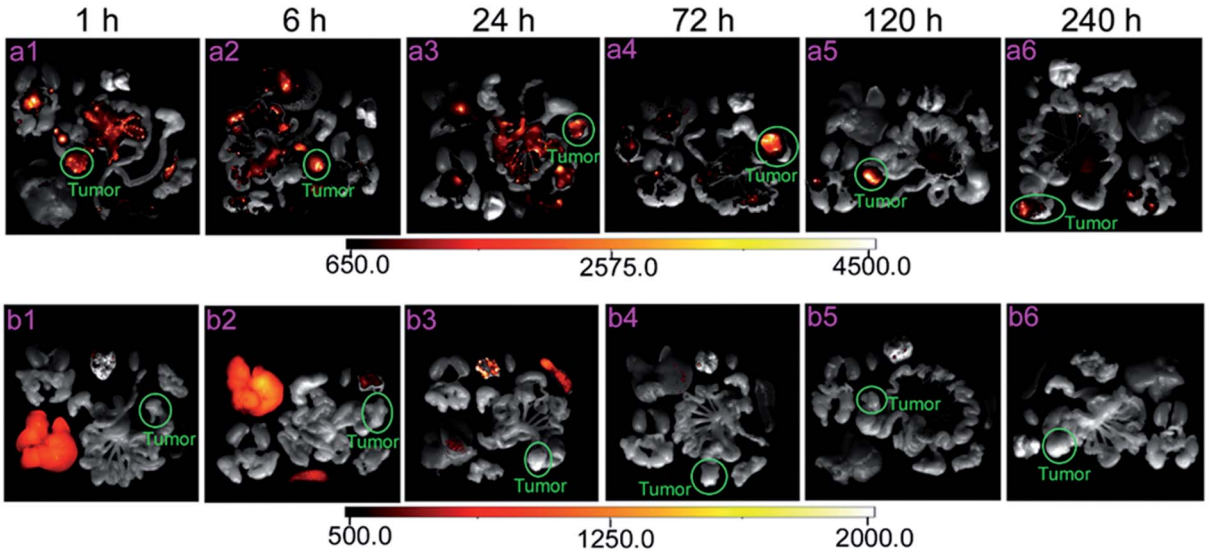

Fig. 6 *Ex vivo* images of the tumours in the colorectal cancer models within 240 h after IP (a1–a6) or IV (b1–b6) injection. Upconversion luminescence signals were collected at 800 ± 12 nm under excitation with CW 980 nm laser.

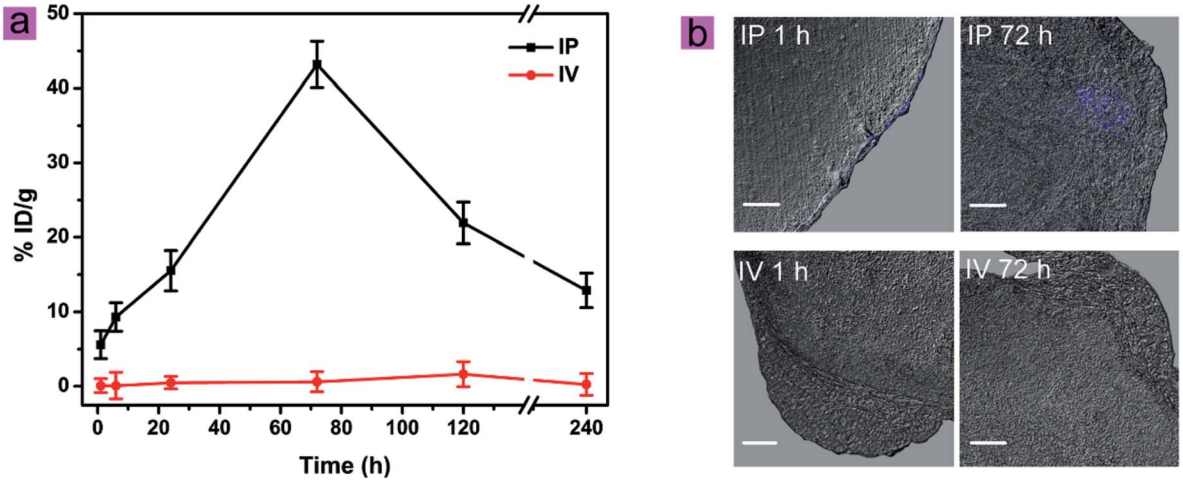

Fig. 7 (a) Comparison of unit mass accumulations (% ID per g) of Lu^{3+} in the tumours of the colorectal cancer models following IP or IV injection of cit-$NaLuF_4$:Yb,Tm@$NaLuF_4$ (16 mg kg^{-1} wt) at various time points (1 h, 6 h, 24 h, 72 h, 120 h and 240 h). (b) Fluorescence distribution in slices of the tumours injected intraperitoneally or intravenously. Upconversion luminescence signals were collected at 400–500 nm under excitation with CW 980 nm laser. Scale bars represented 200 μm.

accumulating amounts of agents in the tumours and less amounts in the mononuclear phagocyte system. However, this administrating way is usually high risky. The intra-muscular administration is appropriate for narcotic analgesics and antibiotics, but it may cause nerve injury.[31] These administration routes should be selected in accordance with the goals of the studies. As for cancer theranostics, especially the tumours locating in the abdominal cavity, the intraperitoneal administration seems to be a sensible choice for agent delivery.

3 Materials and instruments

3.1 Materials

The rare-earth oxides RE_2O_3 (99.999%) (RE = Lu, Yb, Tm) were purchased from Shanghai Yuelong New Materials Co., Ltd. Oleylamine (OM, >80%), oleic acids (OA, >90%) and citrates were purchased from Alfa Aesar Ltd. Hydrochloric acid, cyclohexane and ethanol were obtained from Sinopharm Chemical Reagent Co., Ltd (SCRC). Roswell Park Memorial Institute's medium (RPMI) 1640 culture solution was bought from Hangzhou Jinuo Biomedical Co., Ltd. Rare-earth chloride solutions were prepared as described. Deionized water was employed throughout. All the other reagents were analytical and dealed without further purification.

3.2 Characterization

The size and morphology of as-prepared nanoparticles were determined by transmission electron microscope (TEM, JEOL JEM-2010). Fourier-transform infrared (FTIR) spectra were collected using an IR PRESTIGE-21 spectrometer (Shimadzu) from samples in KBr pellets. X-ray powder diffraction (XRD) measurements were accomplished with a Bruker D4X-ray diffractometer (Cu Kα radiation, λ = 0.15406 nm). An Edinburgh LFS-920 spectrometer, of which the xenon lamp was replace with the external 0–3 W adjustable CW laser at 980 nm (Connet Fiber Optics, China), was used to measure UCL spectra of the as-prepared nanoparticles.

3.3 Synthesis and characterization of $NaLuF_4$:Yb,Tm@$NaLuF_4$ nanocrystals modified with citrates

$NaLuF_4$:Yb,Tm nanoparticles were synthesized in a solvothermal method.[32] The core/shell structured $NaLuF_4$:Yb,Tm@$NaLuF_4$ was prepared with an epitaxial growth method.[33] Citrates modified core–shell nanoparticles were prepared in accordance with the previously reported literature.[34,35]

3.4 Animals protocols

All animal experiments were performed in compliance with the guidelines of National Institute for Food and Drug Control, China, and were approved by the Institutional Animal Care and Use Committee, School of Pharmacy, Fudan University. Kunming male mice (4 weeks old, 18–21 g body weight) were purchased from the Second Military Medical University and used in this study. Male colorectal cancer models, developed with human colorectal cancer LOVO cell line, were purchased from SLRC Laboratory Animal Co., Ltd (Shanghai, China). The tumours were grown to 3–4 mm in diameter. The mice were fed in a temperature-controlled, light cycled room. Cit-UCNPs were injected into the mice at a dosage of 16 mg kg^{-1} body weight. IP injection was inserted into the abdominal cavity, while IV injection, which was served as the contrast test, was through tail vein of mice.

3.5 Absorption, distribution, metabolism and excretion of cit-UCNPs in normal mice

Before the ADME (absorption, distribution, metabolism and excretion) analysis, the luminescence intensity of the synthesized cit-UCNPs dispersed in aqueous solution was detected with *in vivo* imaging system (*In Vivo* Xtreme, designed by our

group). Upon irradiation by a CW 980 nm laser with a power density of 50 mW cm^{-2}, upconversion luminescence signals of 800 ± 12 nm were collected and the related data were analyzed with Kodak Molecular Imaging Software. When the counts of cit-UCNPs at 800 nm were about 3000, the concentration of the nanomaterials could serve as the lowest working concentration in animal experiments. The cit-UCNPs at such concentration in 50 μL volume were injected into mice *via* the intraperitoneal or intravenous route. In this study, 16 mg kg^{-1} wt was the lowest injecting dosage for the cit-UCNPs to successfully perform upconversion luminescence imaging *in vivo*.

UCL imaging was used to study distribution of cit-UCNPs in Kunming male mice given an IP or IV injection. The injected mice were fed in special metabolic cages. At 1 h, 6 h, 12 h, 24 h, 48 h, 72 h, 120 h and 240 h, feces and urine of three normal mice per time point were collected for quantitative detection. Then, these mice were sacrificed and anatomized at each time point. Under the excitation at 980 nm, UCL signals at 800 ± 12 nm were collected and images were analyzed. Furthermore, the tissues of the mice, including the heart, the lung, the liver, the spleen, the intestines, the stomach, the pancreas, the reproductive system, the peritoneum, the mesentery and the kidneys, were weighed and subsequently digested in HNO_3 for 12 h at 60 °C. The digested solutions were diluted with deionized water. ICP-AES assay for Lu^{3+} concentration of the samples was performed and validated. The ICP-AES protocol was provided by Research Centre for Analysis & Measurement, Fudan University. The samples, along with a set of calibration samples, were then run on a P-4010 inductively coupled plasma atomic emission spectrometer (Hitachi Limited, Japan). Unit mass accumulations of Lu^{3+}, expressed as the percentage of dose per gram (% ID per g), was calculated by comparing the amount of Lu^{3+} in certain tissues with standard of injected dose (ID).[36–38] The corresponding values were evaluated as mean ± standard deviation for three mice per group.

3.6 UCL confocal imaging of main organs

Histological section analysis was performed as previously described.[39] 5 μm cryostat sections of the frozen tissues were imaged by laser scanning upconversion luminescence microscopy (LSUCLM) with an Olympus FV1000 scanning unit. Upon excitation at 980 nm, luminescence signals were collected in the channel of 400–500 nm.

3.7 Biosafety assessment of cit-UCNPs at the dosage used for UCL imaging *in vivo*

Each of Kunming male mice was injected intraperitoneally with cit-UCNPs at 16 mg kg^{-1} wt, while mice in the control group were treated with none ($n = 6$). At 24 h and 60 d post-injection, blood of the mice under treatment was collected for serology studies. After that, the mice were sacrificed and the organs (the liver, the spleen, the lung, the kidneys and the pancreas) were recovered.

The blood in 500 μL, collected in microtubes containing ethylene diamine tetraacetic acids, was tested for routine hematological assay.[40,41] The parameters contained white blood cell (WBC), neutrophil (NEUT), mononuclear macrophage (MONO), eosinophile granulocyte (EO), lymphocyte (LYMPH), red blood cell (RBC), *etc.* In addition, each of blood samples in 600 μL was centrifuged at 2000 rpm for 10 min at ambient temperature after keeping stationary for 0.5 h. The sera were separated in order to evaluate the liver and the renal function. These indices contained aspartate transaminase (AST), alanine transaminase (ALT), alkaline phosphatase (ALP), total bilirubin (T-BIL), globulin (GLOB), albumin (ALB), total protein (TP), creatinine (CRE), uric acid (UA) and blood urea nitrogen (BUN).

In order to further examine the possible toxicity *in vivo* induced by IP treatments, the harvested organs underwent histopathology analysis, involving general aspects of organ preservation, nuclear pyknosis, inflammatory infiltrate, cell desquamation, *etc.*[35]

3.8 Tumour accumulation of cit-UCNPs in colorectal cancer models

Tumour-bearing male mice were euthanized at 1 h, 6 h, 24 h, 72 h, 120 h and 240 h after injection with cit-UCNPs *via* the IP or IV route ($n = 3$). The harvested tumours and main organs containing the liver, the spleen, the intestines, the kidneys and the lung were imaged. Afterwards, collected and digested in HNO_3 for 12 h at 60 °C, the tissues were diluted with deionized water and detected by ICP-AES. The passive tumour-targeting efficiency of cit-UCNPs was assessed by % ID per g.[42,43] In addition, histological section analysis was performed.

3.9 Statistics

Given as mean ± standard deviation for at least three repetitions, the results were examined by paired Student's *t* test. *P* values of less than 5% were considered significant difference, and less than 1% were highly significant difference.[44]

4 Conclusions

In the present study, core–shell nanocomposites $NaLuF_4$:Yb,Tm@$NaLuF_4$, modified with citrates, were prepared and subsequently injected *via* the IP route into the normal male mice for basic biological research. The relevant results indicated that cit-UCNPs *via* IP injection could predominantly accumulate in the regional and local tissues in the abdominal cavity, which led to quite different biodistribution and metabolism from that *via* IV injection. It is at relatively faster rate that UCNPs in the IP group were cleared away from body than that in the IV group. More importantly, the passive tumour-targeting effectiveness of cit-UCNPs *via* the IP route was evaluated, and the results indicated that UCNPs *via* the IP route had significantly higher tumour-targeting efficiency than that *via* the IV route. A thorough comprehension – biological processes of UCNPs through IP injection, and the unique advantage in passively targeting to the tumour in colorectal cancer *in situ* – might not only guide excellent design of nanoparticles, but also elevate UCNPs-based treatment from a promising field to a viable and practical strategy for disease in the clinical arena.

Acknowledgements

The authors acknowledge the financial support from the National Natural Science Foundation of China (21231004).

Notes and references

1 C. Liu, Y. Qi, R. Qiao, Y. Hou, K. Chan, Z. Li, J. Huang, L. Jing, J. Du and M. Gao, Detection of early primary colorectal cancer with upconversion luminescent NP-based molecular probes, *Nanoscale*, 2016, **8**(25), 12579–12587.

2 H. Matsuzaki, M. Kamiya, R. J. Iwatate, D. Asanuma, T. Watanabe and Y. Urano, Novel Hexosaminidase-Targeting Fluorescence Probe for Visualizing Human Colorectal Cancer, *Bioconjugate Chem.*, 2016, **27**(4), 973–981.

3 R. Nishihara, K. Wu, P. Lochhead, T. Morikawa, X. Liao, Z. R. Qian, K. Inamura, S. A. Kim, A. Kuchiba, M. Yamauchi, Y. Imamura, W. C. Willett, B. A. Rosner, C. S. Fuchs, E. Giovannucci, S. Ogino and A. T. Chan, Long-term colorectal-cancer incidence and mortality after lower endoscopy, *N. Engl. J. Med.*, 2013, **369**(12), 1095–1105.

4 A. Shaukat, S. J. Mongin, M. S. Geisser, F. A. Lederle, J. H. Bond, J. S. Mandel and T. R. Church, Long-term mortality after screening for colorectal cancer, *N. Engl. J. Med.*, 2013, **369**(12), 1106–1114.

5 H. J. Han, H. B. Wang, Y. J. Chen, Z. H. Li, Y. Wang, Q. Jin and J. Ji, Theranostic reduction-sensitive gemcitabine prodrug micelles for near-infrared imaging and pancreatic cancer therapy, *Nanoscale*, 2016, **8**, 283–291.

6 Y. Zhang, H. Hong, B. Sun, K. Carter, Y. Qin, W. Wei, D. Wang, M. Jeon, J. Geng, R. J. Nickles, G. Chen, P. N. Prasad, C. Kim, J. Xia, W. Cai and J. F. Lovell, Surfactant-stripped Naphthalocyanines for Multimodal Tumor Theranostics with Upconversion Guidance Cream, *Nanoscale*, 2017, **9**(10), 3391–3398.

7 A. Nadort, J. Zhao and E. M. Goldys, Lanthanide upconversion luminescence at the nanoscale: fundamentals and optical properties, *Nanoscale*, 2016, **8**(27), 13099–13130.

8 J. Y. Han, H. P. Xia, Y. F. Wu, S. N. Kong, A. Deivasigamani, R. Xu, K. M. Hui and Y. J. Kang, Single-layer MoS_2 nanosheet grafted upconversion nanoparticles for near-infrared fluorescence imaging-guided deep tissue cancer phototherapy, *Nanoscale*, 2016, **8**, 7861–7865.

9 H. Kim, K. Chung, S. Lee, D. H. Kim and H. Lee, Near-infrared light-responsive nanomaterials for cancer theranostics, *Wiley Interdiscip. Rev.: Nanomed. Nanobiotechnol.*, 2016, **8**(1), 23–45.

10 G. Chen, J. Shen, T. Y. Ohulchanskyy, N. J. Patel, A. Kutikov, Z. Li, J. Song, R. K. Pandey, H. Agren, P. N. Prasad and G. Han, (alpha-$NaYbF_4$:Tm(3+))/CaF_2 core/shell nanoparticles with efficient near-infrared to near-infrared upconversion for high-contrast deep tissue bioimaging, *ACS Nano*, 2012, **6**(9), 8280–8287.

11 Y. Yang, Y. Sun, T. Cao, J. Peng, Y. Liu, Y. Wu, W. Feng, Y. Zhang and F. Li, Hydrothermal synthesis of $NaLuF_4$:^{153}Sm,Yb,Tm nanoparticles and their application in dual-modality upconversion luminescence and SPECT bioimaging, *Biomaterials*, 2013, **34**(3), 774–783.

12 Y. I. Park, K. T. Lee, Y. D. Suh and T. Hyeon, Upconverting nanoparticles: a versatile platform for wide-field two-photon microscopy and multi-modal *in vivo* imaging, *Chem. Soc. Rev.*, 2015, **44**(6), 1302–1317.

13 S. Y. Xu, S. Huang, Q. He and L. Y. Wang, Upconversion nanophosphores for bioimaging, *Trends Anal. Chem.*, 2015, **66**, 72–79.

14 B. Tian, Q. Wang, Q. Su, W. Feng and F. Li, *In vivo* biodistribution and toxicity assessment of triplet–triplet annihilation-based upconversion nanocapsules, *Biomaterials*, 2017, **112**, 10–19.

15 Z. Liu, Z. Li, J. Liu, S. Gu, Q. Yuan, J. Ren and X. Qu, Long-circulating Er^{3+}-doped Yb_2O_3 up-conversion nanoparticle as an *in vivo* X-Ray CT imaging contrast agent, *Biomaterials*, 2012, **33**(28), 6748–6757.

16 K. Kristensen, A. J. Urquhart, E. Thormann and T. L. Andresen, Binding of human serum albumin to PEGylated liposomes: insights into binding numbers and dynamics by fluorescence correlation spectroscopy, *Nanoscale*, 2016, **8**(47), 19726–19736.

17 M. Tsai, Z. Lu, J. Wang, T. K. Yeh, M. G. Wientjes and J. L. Au, Effects of carrier on disposition and antitumor activity of intraperitoneal Paclitaxel, *Pharm. Res.*, 2007, **24**(9), 1691–1701.

18 W. P. Ceelen and M. F. Flessner, Intraperitoneal therapy for peritoneal tumors: biophysics and clinical evidence, *Nat. Rev. Clin. Oncol.*, 2010, **7**(2), 108–115.

19 P. Petignat, A. du Bois, I. Bruchim, D. Fink and D. M. Provencher, Should intraperitoneal chemotherapy be considered as standard first-line treatment in advanced stage ovarian cancer?, *Crit. Rev. Oncol. Hematol.*, 2007, **62**(2), 137–147.

20 D. Curry, A. Cameron, B. MacDonald, C. Nganou, H. Scheller, J. Marsh, S. Beale, M. Lu, Z. Shan, R. Kaliaperumal, H. Xu, M. Servos, C. Bennett, S. MacQuarrie, K. D. Oakes, M. Mkandawire and X. Zhang, Adsorption of doxorubicin on citrate-capped gold nanoparticles: insights into engineering potent chemotherapeutic delivery systems, *Nanoscale*, 2015, **7**(46), 19611–19619.

21 V. Bastos, J. M. Ferreira-de-Oliveira, J. Carrola, A. L. Daniel-da-Silva, I. F. Duarte, C. Santos and H. Oliveira, Coating independent cytotoxicity of citrate- and PEG-coated silver nanoparticles on a human hepatoma cell line, *J. Environ. Sci.*, 2017, **51**, 191–201.

22 J. Grimm, A. Potthast, A. Wunder and A. Moore, Magnetic resonance imaging of the pancreas and pancreatic tumors in a mouse orthotopic model of human cancer, *Int. J. Cancer*, 2003, **106**(5), 806–811.

23 R. J. Holbrook, N. Rammohan, M. W. Rotz, K. W. MacRenaris, A. T. Preslar and T. J. Meade, Gd(III)–Dithiolane Gold Nanoparticles for T1-Weighted Magnetic Resonance Imaging of the Pancreas, *Nano Lett.*, 2016, **16**(5), 3202–3209.

24 B. C. Lucey, J. W. Stuhlfaut and J. A. Soto, Mesenteric Lymph Nodes: Detection and Significance on MDCT., *AJR, Am. J. Roentgenol.*, 2005, **184**(184), 41–44.

25 M. L. Wu, L. Gong, C. Qian, Z. G. Liang and W. Zeng, Characteristics of blood chemistry, hematology, and lymphocyte subsets in pregnant rhesus monkeys, *Chin. J. Nat. Med.*, 2015, **13**(6), 409–414.

26 I. Całkosiński, J. Rosińczuk-Tonderys, K. Dzierzba, J. Bazan, M. Całkosińska, J. Majda, M. Dobrzyński and A. Bronowicka-Szydełko, Mechlorethamine (NTG) effects on the erythrocytic and leukocytic blood parameters during experimentally induced pleuritis in rats, *Pharmacol. Rep.*, 2012, **64**(3), 650–672.

27 L. Xiong, T. Yang, Y. Yang, C. Xu and F. Li, Long-term *in vivo* biodistribution imaging and toxicity of polyacrylic acid-coated upconversion nanophosphors, *Biomaterials*, 2010, **31**(27), 7078–7085.

28 A. R. Fernandes, J. Jesus, P. Martins, S. Figueiredo, D. Rosa, L. M. Martins, M. L. Corvo, M. C. Carvalheiro, P. M. Costa and P. V. Baptista, Multifunctional gold-nanoparticles: A nanovectorization tool for the targeted delivery of novel chemotherapeutic agents, *J. Controlled Release*, 2017, **245**, 52–61.

29 A. H. Silva, C. Locatelli, F. B. Filippin-Monteiro, P. Martin, N. J. Liptrott, B. G. Zanetti-Ramos, L. C. Benetti, E. M. Nazari, C. A. Albuquerque, A. A. Pasa, A. Owen and T. B. Creczynski-Pasa, Toxicity and inflammatory response in Swiss albino mice after intraperitoneal and oral administration of polyurethane nanoparticles, *Toxicol. Lett.*, 2016, **246**, 17–27.

30 X. Zhu, R. B. Da Silva, X. Zou, B. Shen, Y. Sun, W. Feng and F. Li, Intra-arterial infusion of PEGylated upconversion nanophosphors to improve the initial uptake by tumors *in vivo*, *RSC Adv.*, 2014, **4**(45), 23580–23584.

31 M. T. Hdaib, S. M. Al-Momany and Y. W. Najjar, Knowledge level assessment and change among nursing students regarding administering intra-muscular injection at Al-Balqa'a Applied University: an interventional study, *Nurse Educ Today.*, 2015, **35**(7), 18–22.

32 Z. Chen, Z. Liu, Z. Li, E. Ju, N. Gao, L. Zhou, J. Ren and X. Qu, Upconversion nanoprobes for efficiently *in vitro* imaging reactive oxygen species and *in vivo* diagnosing rheumatoid arthritis, *Biomaterials*, 2015, **39**, 15–22.

33 L. Zhao, J. Peng, Q. Huang, C. Li, M. Chen, Y. Sun, Q. Lin, L. Zhu and F. Li, Near-Infrared Photoregulated Drug Release in Living Tumor Tissue *via* Yolk–Shell Upconversion Nanocages, *Adv. Funct. Mater.*, 2014, **24**(3), 363–371.

34 P. F. Cao, Y. H. Yan, J. D. Mangadlao, L. H. Rong and R. Advincula, Star-like copolymer stabilized noble-metal nanoparticle powders, *Nanoscale*, 2016, **8**(14), 7435–7442.

35 J. Peng, Y. Sun, L. Zhao, Y. Wu, W. Feng, Y. Gao and F. Li, Polyphosphoric acid capping radioactive/upconverting $NaLuF_4$:Yb,Tm,^{153}Sm nanoparticles for blood pool imaging *in vivo*, *Biomaterials*, 2013, **34**(37), 9535–9544.

36 V. L. Dressler, F. G. Antes, C. M. Moreira, D. Pozebon and F. A. Duarte, As, Hg, I, Sb, Se and Sn speciation in body fluids and biological tissues using hyphenated-ICP-MS techniques: A review, *Int. J. Mass Spectrom.*, 2011, **307**, 149–162.

37 I. Juranovic Cindric, I. Krizman, M. Zeiner, S. Kampic, G. Medunic and G. Stingeder, ICP-AES determination of minor- and major elements in apples after microwave assisted digestion, *Food Chem.*, 2012, **135**(4), 2675–2680.

38 S. Chen, K. Yang, R. G. Tuguntaev, A. Mozhi, J. Zhang, P. C. Wang and X. J. Liang, Targeting tumor microenvironment with PEG-based amphiphilic nanoparticles to overcome chemoresistance, *Nanomedicine: Nanotechnology, Biology and Medicine*, 2016, **12**(2), 269–286.

39 T. Kamei, J. Kitayama, H. Yamaguchi, D. Soma, S. Emoto, T. Konno, K. Ishihara, H. Ishigami, S. Kaisaki and H. Nagawa, Spatial distribution of intraperitoneally administrated paclitaxel nanoparticles solubilized with poly(2-methacryloxyethyl phosphorylcholine-*co*-*n*-butyl methacrylate) in peritoneal metastatic nodules, *Cancer Sci.*, 2011, **102**(1), 200–205.

40 X. D. Zhang, H. Y. Wu, D. Wu, Y. Y. Wang, J. H. Chang, Z. B. Zhai, A. M. Meng, P. X. Liu, L. A. Zhang and F. Y. Fan, Toxicologic effects of gold nanoparticles *in vivo* by different administration routes, *Int. J. Nanomed.*, 2010, **5**, 771–781.

41 S. Xu, H. Fan, L. Yin, J. Zhang, A. Dong, L. Deng and H. Tang, Thermosensitive hydrogel system assembled by PTX-loaded copolymer nanoparticles for sustained intraperitoneal chemotherapy of peritoneal carcinomatosis, *Eur. J. Pharm. Biopharm.*, 2016, **104**, 251–259.

42 C. Zhang, L. Zhou, J. Zhang, Y. Y. Fu, X. Zhang, C. Yu, S. K. Sun and X. P. Yan, Green and facile synthesis of a theranostic nanoprobe with intrinsic biosafety and targeting abilities, *Nanoscale*, 2016, **8**(36), 16204–16211.

43 J. Merian, R. De Souza, Y. Dou, S. N. Ekdawi, F. Ravenelle and C. Allen, Development of a liposome formulation for improved biodistribution and tumor accumulation of pentamidine for oncology applications, *Int. J. Pharm.*, 2015, **488**(1–2), 154–164.

44 T. Wang, D. Wang, H. Yu, M. Wang, J. Liu, B. Feng, F. Zhou, Q. Yin, Z. Zhang, Y. Huang and Y. Li, Intracellularly Acid-Switchable Multifunctional Micelles for Combinational Photo/Chemotherapy of the Drug-Resistant Tumor, *ACS Nano*, 2016.

